

# Synthesis and Cerebral Uptake of 1-(1-[<sup>11</sup>C]Methyl-1*H*-pyrrol-2-yl)-2-phenyl-2-(1-pyrrolidinyl)ethanone, a Novel Tracer for Positron Emission Tomography Studies of Monoamine Oxidase Type A

Svend Borup Jensen,<sup>\*,†</sup> Roberto Di Santo,<sup>\*,‡</sup> Aage Kristian Olsen,<sup>†</sup> Kasper Pedersen,<sup>†</sup> Roberta Costi,<sup>‡</sup> Roberto Cirilli,<sup>§</sup> and Paul Cumming<sup>†</sup>

PET Centre, Aarhus University Hospital, Nørrebrogade 44, 8000 Århus C, Denmark, Istituto Pasteur—Fondazione Cenci Bolognetti, Dipartimento di Studi Farmaceutici, Università di Roma “La Sapienza”, P. le A. Moro 5, I-00185 Roma, Italy, and Dipartimento del Farmaco, Istituto Superiore di Sanità, Viale Regina Elena 299, 00161 Roma, Italy

Received August 13, 2007

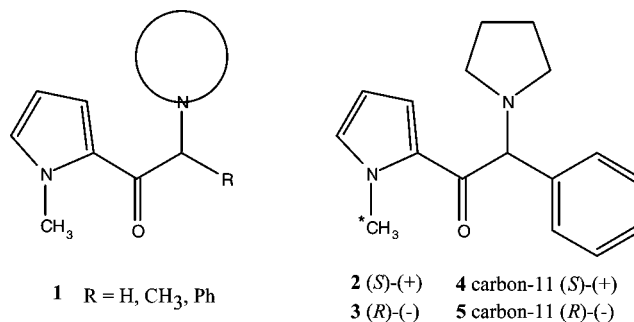
(*R*)-(–)- and (*S*)-(+)-1-(1-[<sup>11</sup>C]methyl-1*H*-pyrrol-2-yl)-2-phenyl-2-(1-pyrrolidinyl)ethanone **4** and **5** were synthesized, and their properties as tracers for positron emission tomography (PET) studies of monoamine oxidase type A (MAO-A) in the brain of living pigs were tested. Parametric maps of the distribution volume ( $V_d$ ) **4** in pig brain were qualitatively similar to those obtained with [<sup>11</sup>C]harmine, with prominent binding in the ventral forebrain and mesencephalon. Its binding was highly vulnerable to MAO blockade, suggesting a binding potential as high as 2 for MAO-A sites. The slow plasma metabolism of **4** and **5** may present advantages over [<sup>11</sup>C]harmine for routine PET studies of MAO-A.

## Introduction

Monoamine oxidase (MAO, EC 1.4.3.4) types A and B are flavin-containing enzymes that contribute importantly to the catabolism of dopamine and other biogenic primary monoamines in the brain.<sup>1</sup> The discovery of the antidepressant property of the irreversible MAO-inhibitor *N'*-propan-2-ylpyridine-4-carbohydrazide (iproniazid) was an early breakthrough in psychopharmacology.<sup>2</sup> However, there have been relatively few ligands suitable for studies of MAO by positron emission tomography (PET). The propargylamine-compound [<sup>11</sup>C *N*-methyl]*N*-[3-(2,4-dichlorophenoxy)propyl]-*N*-methyl-prop-2-yn-1-amine ([<sup>11</sup>C]clorgyline) is a suicide MAO substrate with considerable selectivity for MAO-A,<sup>3,4</sup> and [<sup>11</sup>C *N*-methyl]*N*-methyl-*N*-(1-methyl-2-phenyl-ethyl)-prop-2-yn-1-amine ([<sup>11</sup>C]deprenyl) is an irreversible inhibitor of MAO-B in living brain.<sup>5,6</sup> However, the kinetic analysis of the cerebral binding of these propargylamine ligands is hampered by the very high net clearance from brain and rapid irreversible binding to MAOs, such that net clearance from the brain approaches the limit imposed by cerebral perfusion. Deuterium substitution of the  $\alpha$ -carbon of [<sup>11</sup>C]deprenyl results in a slower rate of association with the MAO-B, which is more favorable for kinetic analysis.<sup>7,8</sup> However, for reasons that remain uncertain, the deuterated derivative of [<sup>11</sup>C]clorgyline yields cerebral-binding maps endowed with relatively poorer contrast between regions of low and high MAO-A activity than those produced by [<sup>11</sup>C]clorgyline itself.<sup>8,9</sup> Several clorgyline analogues synthesized for PET or SPECT (<sup>11</sup>C-fluoroclogyline,<sup>10</sup> <sup>18</sup>F-fluoroclogyline,<sup>11,12</sup> and [<sup>125</sup>I]iodoclogyline) showed low cerebral uptake.<sup>13</sup>

One of the best-characterized reversible PET ligands for imaging MAO-A is [<sup>11</sup>C-MeO]7-MeO-1-Me-9*H*-pyrido[3,4-*b*]indole ([<sup>11</sup>C]harmine, a  $\beta$ -carboline alkaloid, which has been employed in both preclinical studies on animals<sup>14–16</sup> and a

**Chart 1.** Pyrrolyletanoneamines **1–3** Endowed with Potent Activities against MAOs and Newly Designed PET Tracers **4** and **5**<sup>a</sup>



<sup>a</sup> The position with the asterisk shows that the ligands have been labeled with carbon-11.

clinical study of depression in humans).<sup>17</sup> This tracer is very rapidly metabolized in peripheral tissues (only 10% of the plasma radioactivity remains as untransformed [<sup>11</sup>C]harmine at 10 min), which can be an encumbrance to the quantification of its cerebral binding. Another MAO-A PET ligand, [<sup>11</sup>C-1](5*R*)-5-(methoxymethyl)-3-[4-[(3*R*)-4,4,4-trifluoro-3-hydroxybutoxy]phenyl]-2-oxazolidinone ([<sup>11</sup>C]befloxatone), is characterized by relatively slower peripheral metabolism.<sup>18,19</sup> However, [<sup>11</sup>C]befloxatone is synthesized via [<sup>11</sup>C]phosgene, a dangerous reagent available only at a few PET centers.

The lack of an ideal ligand and the emerging importance of MAO-A in PET studies of depression<sup>17</sup> and tobacco addiction<sup>20,21</sup> justify the continued search for a ligand with optimal properties.

Recently, we designed and synthesized a series of pyrrolyletanoneamines (general structure **1**; Chart 1) that showed potent activities as MAO inhibitors, as well as high selectivity against

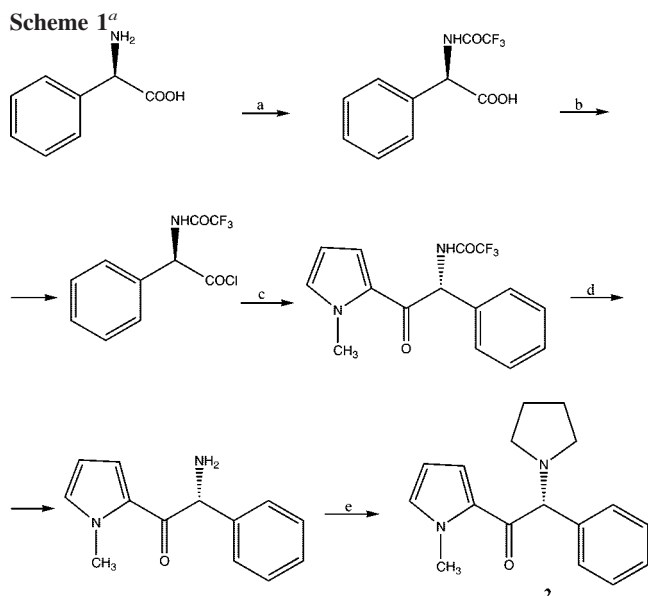
\* To whom correspondence should be addressed. Telephone: +45-8949-3034. Fax: +45-8949-3020. E-mail: svend@pet.auh.dk (S.B.J.); Telephone/Fax: +39-6-49913150. E-mail: roberto.disanto@uniroma1.it (R.D.S.).

<sup>†</sup> Aarhus University Hospital.

<sup>‡</sup> Università di Roma “La Sapienza”.

<sup>§</sup> Istituto Superiore di Sanità.

<sup>a</sup> Abbreviations:  $V_d$ , distribution volume;  $t_0$ , dead time of the column;  $\alpha$ , enantioselectivity; CSP, chiral stationary phase;  $C_a(T)$ , arterial input function; PR(*t*), total plasma radioactivity; PPR(*t*), plasma precipitate radioactivity;  $f_{\text{tracer}}$ , unmetabolized parent radioligand.



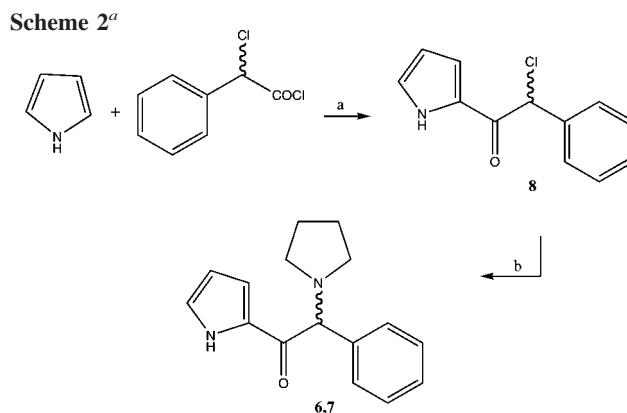
<sup>a</sup> Reagents and conditions for the synthesis of isomer **2**: (a)  $\text{CF}_3\text{COOC}_2\text{H}_5$ , tetramethyl-guanidine, MeOH, room temperature for 24 h, 93%, (b) Vilsmeier reagent, *n*-butyl acetate,  $-15^\circ\text{C}$  for 3 h, (c) 1-methylpyrrole,  $\text{AlCl}_3$ ,  $\text{CH}_2\text{Cl}_2$ ,  $-5^\circ\text{C}$  for 2 h, 13%, (d) concentrated HCl, MeOH,  $40^\circ\text{C}$  for 15 h, 80%, and (e) 1,4-dibromobutane, NaI,  $\text{K}_2\text{CO}_3$ , reflux, 12 h, 67%. The same conditions were used to synthesize the isomer **3**, using (*S*)-phenylglycine as the starting material.

MAO type A. This selectivity was demonstrated against the two specific isoforms on MAO in a mitochondrial preparation from bovine brain, according to the method of Basford.<sup>22</sup> Within this series of MAO inhibitors, we identified (*R*)-(-)-1-(1-(1-methyl-1*H*-pyrrol-2-yl)-2-phenyl-2-(1-pyrrolidinyl)ethanone (*R*-ROMAO, **2**) as a candidate for a PET study for MAO-A based on its 200 000-fold selectivity for MAO-A over the B form,<sup>23</sup> exceeding even the 52 000-fold selectivity found of the *S* enantiomer (*S*-ROMAO, **3**). Furthermore, the chemical structure of these compounds is amenable for [<sup>11</sup>C]-labeling (Chart 1). Our strategy to obtain the compounds (*R*)-(-)-1-(1-[<sup>11</sup>C]methyl-1*H*-pyrrol-2-yl)-2-phenyl-2-(1-pyrrolidinyl)ethanone (*R*-[<sup>11</sup>C]ROMAO, **4**) and (*S*)-(+)-1-(1-[<sup>11</sup>C]methyl-1*H*-pyrrol-2-yl)-2-phenyl-2-(1-pyrrolidinyl)ethanone (*S*-[<sup>11</sup>C]ROMAO, **5**) (Chart 1) was based on the synthesis of (*R*)-(-)- and (*S*)-(+)-2-phenyl-1-(1*H*-pyrrol-2-yl)-2-(1-pyrrolidinyl)ethanone (**6** and **7**), which underwent a [<sup>11</sup>C]-methylation on position 1 of the pyrrole ring to afford the required labeled derivatives **4** and **5**.

We have obtained more than a decade of experience with the pig as an animal for preclinical investigations of radioligands targeted at neurotransmitter systems.<sup>24–26</sup> The large volume of the pig brain (75 mL) is sufficient for the discernment of the anatomical structure by PET, and we have already described in some detail the spatial pattern of binding of [<sup>11</sup>C]harmine to MAO-A in the brain of living pig.<sup>16</sup> In the present study, we tested the plasma metabolism and cerebral uptake of **4** and **5** in anesthetized pigs. Specificity of the binding of *R*-[<sup>11</sup>C]ROMAO in pig brain was tested in a blocking study performed by the pretreatment of the animal with pargyline at a dose known to block MAO-A in pig brain, 1 h before the tracer administration.

## Results and Discussion

**Chemistry.** The syntheses of (*R*)-(-)- and (*S*)-(+)-1-(1-methyl-1*H*-pyrrol-2-yl)-2-phenyl-2-(1-pyrrolidinyl)ethanone (*R*- and *S*-ROMAO, **2** and **3**; Scheme 1) have been described previously.<sup>23</sup>



<sup>a</sup> Reagents and conditions: (a)  $\text{AlCl}_3$ ,  $\text{CH}_2\text{Cl}_2$ ,  $-20^\circ\text{C}$  for 20 min and (b) pyrrolidine,  $\text{K}_2\text{CO}_3$ , acetone, reflux for 96 h.

This synthetic pathway was not immediately transferable to the synthesis of (*R*)-(-)- and (*S*)-(+)-2-phenyl-1-(1*H*-pyrrol-2-yl)-2-(1-pyrrolidinyl)ethanone (desmethyl-*R*- and *S*-ROMAO, **6** and **7**). Derivatives **6** and **7** were therefore obtained as described in Scheme 2. The 1*H*-pyrrole underwent a Friedel–Crafts reaction with 2-chloro-2-phenylacetyl chloride to give 2-chloro-2-phenyl-1-(1*H*-pyrrol-2-yl)ethanone **8** in 20% yield. This compound was treated with pyrrolidine in refluxing acetone using  $\text{K}_2\text{CO}_3$  as a base, to obtain **6** and **7** in 20% yield. The racemic mixture was separated by enantioselective high-performance liquid chromatography (HPLC) at a semipreparative scale on a polysaccharide-based chiral stationary phase (CSP<sup>®</sup>) (Chiralpack IA) to obtain the enantiomers **6** and **7** (80–90% yield) with enantiomeric excess (ee) > 99%, checked by an analytical Chiralpack IA column (Figure 1).

Although the racemic mixture **6** and **7** was obtained in only about 4% global yield, no efforts were made to improve this yield, because the optimization of the synthesis was deemed beyond the scope of the present study.

**Stereochemical Characterization of the Enantiomers **6** and **7**.** The absolute configuration of **6** and **7** was assigned by a comparison of their circular dichroism (CD) spectra with those of the structurally related compounds in the ROMAO series (Figure 2). As previously reported,<sup>23,27</sup> the dextrorotatory form **3** displays negative CD bands at around 254 and 319 nm and two positive CD bands at around 229 and 290 nm. The CD profile of the (+)-**7** enantiomer in ethanol is strikingly similar to that of reference compound (*S*)-(+)-ROMAO **3**, while the (-)-**6** enantiomer showed opposite Cotton effects. Therefore, we could empirically assign the *S* configuration to the dextrorotatory enantiomer **7** and the *R* configuration to the levorotatory enantiomer **6**.

**Radiochemistry.** The carbon-11 labeling of compound **6** to obtain *S*-[<sup>11</sup>C]ROMAO (**4**) took 42 min ( $\pm 5$  min) (Scheme 3). The same conditions were applied to transform its enantiomer compound **7** into *R*-[<sup>11</sup>C]ROMAO (**5**). Yields were 1.2 GBq ( $\pm 0.5$  GBq) from 6 to 9 GBq [<sup>11</sup>C]CH<sub>3</sub>I. When the 20 min physical half-life of carbon-11 was taken into account, the calculated yield of the labeling reaction was 60–70%. The products were 99% ( $\pm 1\%$ ) radiochemically pure; the residual content of precursor was below 50  $\mu\text{g}$ /production; and the contents of *S*- or *R*-ROMAO **4** or **5** were below 10  $\mu\text{g}$ /production. The specific activity was higher than 50 GBq/ $\mu\text{mol}$ .

**Metabolic Stability of Carbon-11-Labeled *S*- and *R*-ROMAO (**4** and **5**).** Four pigs were used for both PET scan imaging studies and studies of the plasma metabolism of the carbon-11-labeled *S*- and *R*-ROMAO (**4** and **5**). Each pig was

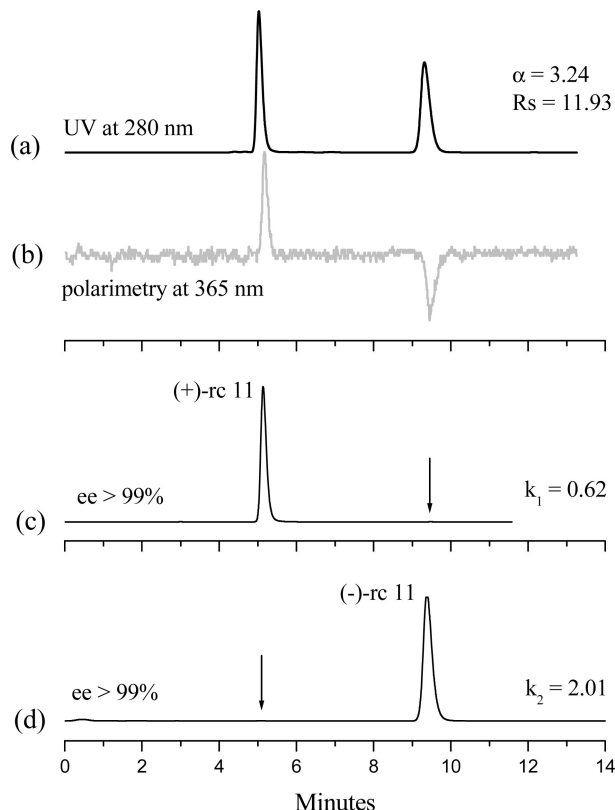


**Figure 1.** (Traces a and b) Analytical separation of desmethyl-ROMAO with UV and polarimetric detection. (Traces c and d) Purity control of the first and second fractions collected at a semipreparative scale.  $k_1$ , retention factor of the first eluted enantiomer, defined as  $(t_1 - t_0)/t_0$ , where  $t_0$  is the dead time of the column.  $\alpha$ , enantioselectivity factor defined as  $k_2/k_1$ .  $R_s$ , resolution factor defined as  $2(t_2 - t_1)/(w_1 + w_2)$ , where  $t_1$  and  $t_2$  are retention times and  $w_1$  and  $w_2$  are band widths at the baseline in time units.

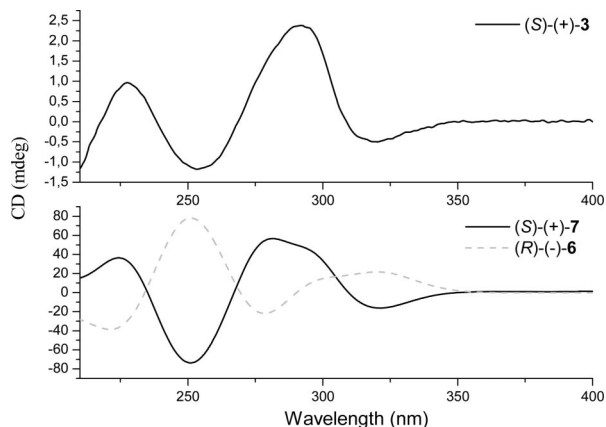
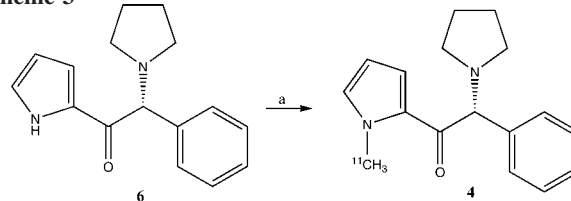


**Figure 2.** CD profiles of reference compound (*S*)-(+)-ROMAO (**3**) and the enantiomers of desmethyl-ROMAO (**6** and **7**) in ethanol.

premedicated and anaesthetised as described in detail previously.<sup>24–26</sup> Catheters had been placed in an femoral artery for blood sampling and in a femoral vein for radiotracer injection. Arterial blood samples were collected at intervals during PET scans for pgs 2, 3, and 4 only for HPLC plasma metabolite measurements. Carbon-11 analogues **4** and **5** were relatively stable toward metabolism in the plasma of living pigs, compared to [<sup>11</sup>C]harmine.<sup>16</sup> Metabolite HPLC analysis of the two stereoisomers shows no notable differences between the two isomers. At 30 s after intravenous injection, 99.7% of the extracted plasma radioactivity was the untransformed parent. This fraction

### Scheme 3<sup>a</sup>



<sup>a</sup> Reagents and conditions: (a) <sup>11</sup>CH<sub>3</sub>I, NaH, DMF, room temperature for 1 min. The same conditions were used to obtain **5** using **7** as the starting material.

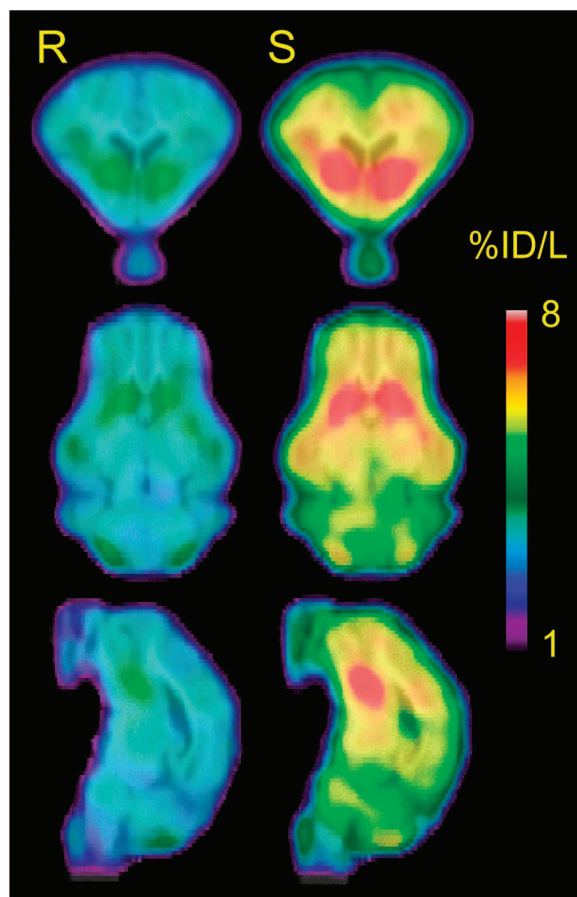


**Figure 3.** Normalized uptake of the *R*- and *S*-[<sup>11</sup>C]ROMAO **4** and **5** in pig brain. The values are the average concentrations of the interval between 10 and 60 min, as a percentage of the injected dose per liter (% ID/L). Extracerebral voxels have been removed, and the images are blurred (4 mm fwhm). Maps are shown in coronal, sagittal, and horizontal planes.

declined to 98% at 2 min, 68% at 10 min, 41% at 30 min, and 24% untransformed at 50 min. Reverse-phase radio-HPLC analysis of the plasma showed that the radio-metabolite(s) eluted early in the radiochromatogram, indicating that radio-metabolite(s) are considerably more polar than the parent compound. This predicts that the metabolites do not enter the brain,<sup>28</sup> which is a precondition for kinetic modeling. Consequently, no attempt was made to identify the polar plasma metabolites.

**PET Examination of *R*- and *S*-[<sup>11</sup>C]ROMAO **4** and **5**.** The anaesthetised pig was placed in the PET scanner before injection of the radiotracer. On the basis of its higher selectivity for MAO-A, we expected that *R*-[<sup>11</sup>C]ROMAO **4** might have superior binding properties in the living brain when compared to its enantiomer **5**. Contrary to this expectation, maps of the normalized uptake of the two enantiomers in pig brain show that

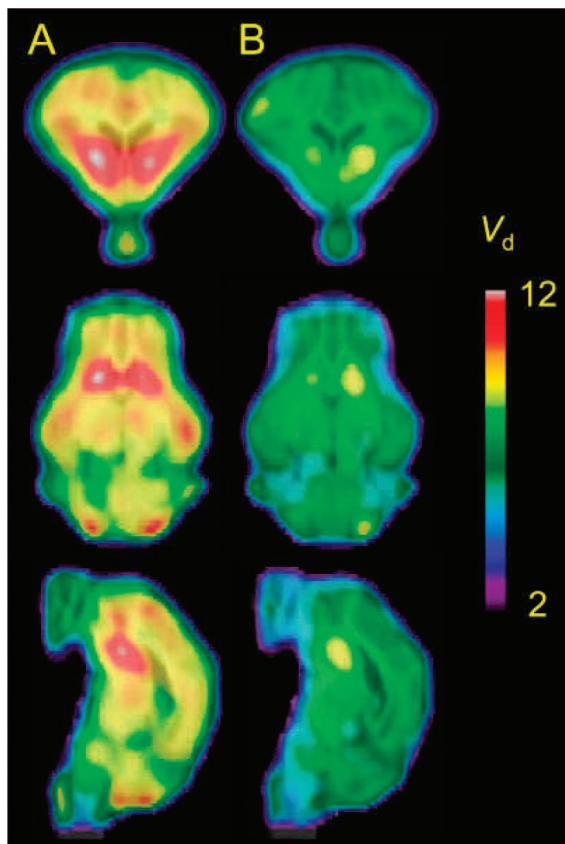


**Figure 4.** Parametric images of  $R$ - $[^{11}\text{C}]$ ROMAO (**4**) distribution volume in pig 4 before (A) and after (B) pargyline. Extracerebral voxels have been removed, and the images are blurred (4 mm). Maps are shown in coronal, sagittal, and horizontal planes.

net uptake of the  $S$  form **5** was 2-fold greater than for the  $R$  form **4** (Figure 3). The specific activities of the two injections were both very high ( $>100$  GBq/ $\mu\text{mol}$ ), and the dose injected was very similar, at 480 MBq ( $\pm 20$  MBq). Compounds **4** and **5** have very similar metabolic patterns; therefore, differences in plasma metabolism cannot explain the higher brain uptake of the  $S$  form compared to the  $R$  form.

Comparison of the parametric maps of the equilibrium distribution volume ( $V_d$ ,  $\text{mL g}^{-1}$ ) relative to the metabolite-corrected arterial input for **4** and **5** ( $R$ - and  $S$ - $[^{11}\text{C}]$ ROMAO) with previously obtained results for  $[^{11}\text{C}]$ harmine<sup>16</sup> showed that all three tracers had preferential radioactivity accumulation in the ventral forebrain/ventral striatum. In the parametric maps of **4** and **5** ( $R$ - and  $S$ - $[^{11}\text{C}]$ ROMAO)  $V_d$  had only this single "hotspot" (Figure 3), in contrast to  $[^{11}\text{C}]$ harmine, which had a somewhat more complex pattern of cerebral binding.

To verify the pharmacological nature of its binding in brain, a blocking PET study was carried out with **4** in pig 4. A baseline recording was followed by a second scan, initiated at 1 h after pargyline treatment (5 mg/kg, i.v.). At intervals after tracer injection, we measured the radioactivity in (i) whole arterial blood, (ii) plasma, and (iii) acetonitrile precipitate of plasma. The extract after acetonitrile precipitation plasma was examined by HPLC to measure the metabolism at selected times. The  $V_d$  maps were calculated as relative to the untransformed tracer in the plasma extracts. The fraction precipitated with acetonitrile was reduced to 25–30% after treatment with pargyline, suggesting that bound  $R$ - $[^{11}\text{C}]$ ROMAO (**4**) can be trapped in a plasma protein compartment by a MAO-dependent process. Taking into account the above, we used the following equation

to generate the arterial input concentration as a function of the circulation time (arterial input function,  $C_a(T)$ ):

$$C_a(T) = \text{PR}(t)[\text{PR}(t) - \text{PPR}(t)/\text{PR}(t)]f_{\text{tracer}} \quad (1)$$

where  $\text{PR}(t)$  is the total plasma radioactivity,  $\text{PPR}(t)$  is the plasma precipitate radioactivity, and  $f_{\text{tracer}}$  is the unmetabolized parent radioligand, measured by radio-HPLC. This equation corrects for both protein binding and metabolism of the free tracer.

The first term of eq 1 referred to the measured plasma radioactivity ( $\text{PR}$ ); the second term  $[\text{PR}(t) - \text{PPR}(t)/\text{PR}(t)]$  takes into account the amount unavailable for brain uptake because of protein binding; and the third term ( $f_{\text{tracer}}$ ) considers the removal of the metabolites from the input function.

In our previous study using  $[^{11}\text{C}]$ harmine to visualize the MAO enzyme, we found that the  $V_d$  in the pituitary gland was partly resistant to pargyline blockage, suggesting some pharmacological heterogeneity in that structure.<sup>16</sup> However,  $[^{11}\text{C}]$ ROMAO (**4** nor **5**) did not discernibly label the pig pituitary; indeed, with  $[^{11}\text{C}]$ ROMAO (**4** or **5**), the only region with distinctly greater binding was the ventral forebrain (Figure 4), although there was some evidence of greater uptake in the diencephalon. The blocking study revealed a global fall in  $V_d$  throughout out the brain, which was most conspicuous in the ventral forebrain, consistent with the global pattern of distribution of MAO-A.

## Conclusions

On the basis of these preliminary results, both  $R$ - and  $S$ - $[^{11}\text{C}]$ ROMAO **4** and **5** appear to be very promising PET tracers for the MAO-A enzyme in brain. There are several positive attributes to these ligands, which may present advantages over  $[^{11}\text{C}]$ harmine and other existing ligands. In particular, the carbon-11-labeling reaction is fairly simple and robust. Yields of more than 1 GBq were routinely obtained and with high specific activity of the final product. The metabolism of  $R$ - and  $S$ - $[^{11}\text{C}]$ ROMAO (**4** and **5**) is relatively slow in plasma of living pigs, in contrast to  $[^{11}\text{C}]$ harmine, which is difficult to detect in plasma at times after 10 min. Parametric maps of  $[^{11}\text{C}]$ ROMAOs **4** and **5** binding are qualitatively very comparable to those of  $[^{11}\text{C}]$ harmine.<sup>16</sup> There was extensive displacement of binding after the blockade of the MAO-A enzyme with pargyline at a dose known to block entirely  $[^{11}\text{C}]$ harmine binding in pig brain.

## Experimental Section

**Chemistry. General.** Melting points were determined with a Buchi 530 capillary apparatus and are uncorrected. Infrared (IR) spectra were recorded on a Spectrum-one spectrophotometer.  $^1\text{H}$  NMR spectra were recorded on a Bruker AC 400 spectrometer, using tetramethylsilane ( $\text{Me}_4\text{Si}$ ) as an internal standard. All compounds were routinely checked by thin-layer chromatography (TLC) and  $^1\text{H}$  nuclear magnetic resonance (NMR). TLC was performed using aluminum-baked silica gel plates (Fluka F<sub>254</sub>) and aluminum-baked aluminum oxide plates (Fluka F<sub>254</sub>). The concentration of solutions after reactions and extractions was obtained using a rotatory evaporator operating at a reduced pressure of approximately 20 Torr. Organic solutions were dried over anhydrous sodium sulfate. Solvents and reagents were obtained from commercial suppliers (Sigma-Aldrich) and were used without further purification.

**Syntheses. 2-Chloro-2-phenyl-1-(1H-pyrrol-2-yl)ethanone (8).**  $\text{AlCl}_3$  (9.9 g, 74.2 mmol) was added in small portions during 30 min into a well-stirred solution of pyrrole (10 g, 149.0 mmol) and 2-chloro-2-phenylacetyl chloride (14.1 g, 74.5 mmol) in  $\text{CH}_2\text{Cl}_2$  (120 mL) cooled at  $-20$  °C. The mixture was stirred at  $-20$  °C for 20 min, and then the mixture was added to a slush consisting

of crushed ice (250 g) and concentrated HCl (17 mL). Extraction with  $\text{CHCl}_3$  ( $3 \times 200$  mL) provided an organic solution that was washed with brine ( $3 \times 250$  mL), saturated  $\text{NaHCO}_3$  solution ( $1 \times 250$  mL), then with brine again ( $3 \times 250$  mL), before it was dried. Removal of the solvent by evaporation yielded a residue, which was chromatographed on an alumina column (chloroform as the eluent) to afford pure **8** (racemic mixture) (3.27 g, 20%). For analytical data, see the Supporting Information.

**2-Phenyl-1-(1*H*-pyrrol-2-yl)-2-(1-pyrrolidinyl)ethanone (6 and 7) (Desmethyl-ROMAO).** A solution of **8** (2.6 g, 11.6 mmol) in acetone (52 mL) was added dropwise into a well-stirred suspension of pyrrolidine (1.6 g, 23.1 mmol) and  $\text{K}_2\text{CO}_3$  (3.0 g, 21.6 mmol) in acetone (52 mL). The mixture was refluxed with stirring for 96 h and then treated with water. After extraction with  $\text{CHCl}_3$  (100 mL), the organic solution was washed with brine ( $5 \times 50$  mL) and dried. Evaporation of the solvent gave a crude product, which was chromatographed on a silica column (5:1 ethyl acetate/chloroform as the eluent) to afford **6** and **7** (racemic mixture) (590 mg, 20%). For analytical data, see the Supporting Information.

**Enantioseparation.** HPLC-grade solvents were supplied by Carlo Erba (Milan, Italy). Diethylamine (DEA) was obtained from Fluka Chemie (Buchs, Switzerland). HPLC enantioseparations were carried out by using a Perkin-Elmer (Norwalk, CT) 200 liquid chromatographic pump equipped with a Rheodine (Cotati, CA) injector with a 20  $\mu\text{L}$  (analytical) or 1 mL (semipreparative) sample loop, a Perkin-Elmer column oven, and a Perkin-Elmer 290 UV detector. The sign of the optical rotations of enantiomers of compounds tested was measured online at a wavelength of 365 nm by a Perkin-Elmer polarimeter model 241 equipped with Hg/Na lamps and a 40  $\mu\text{L}$  flow-cell. The signal was acquired and processed by Clarity (Data Apex, Prague, Czech Republic) software. The chiral analytes were dissolved in ethanol, and their CD spectra were measured in a quartz cell (0.1 cm path length) using a Jasco J-710 spectropolarimeter (Japan Spectroscopic, Tokyo, Japan), maintained thermostatically at 25 °C. The mean spectra from three instrumental scans were calculated as ellipticity values (millidegrees).

Semipreparative enantioseparations of **6** and **7** (desmethyl-ROMAO) were accomplished by HPLC on a polysaccharide-based chiral stationary phase (CSP) column type Chiralpak IA  $250 \times 4.6$  mm I.D., with a mixture of 60:40:1:0.1 *n*-hexane/ethyl acetate/ethanol/DEA (v/v/v/v) as the eluent. The column temperature was set at 25 °C, with a flow rate of 4 mL/min and detection wavelength at 280 nm. After each semipreparative chromatographic run (25 mg), the fractions corresponding to a single enantiomer were pooled and evaporated. The collected fractions of each enantiomer were analyzed by analytical Chiralpak IA chiral columns, with a flow rate at 1.0 mL/min, at 25 °C with UV detection at 280 nm, to determine their enantiomeric excess (ee > 99%). The yields ranged from 80 to 90% (Figure 1).

**Animals, Anesthesia, Surgery, and PET Scanning.** The study procedure was approved by the Danish Experimental Animal Inspectorate. A total of 4 Danish Landrace/Yorkshire pigs (females; 38.25–40.5 kg of body weight; approximately 3 months old) were used. For experimental details, see the Supporting Information.

In three cases, the pigs had been used for other PET-scanning protocols before this study. They had previously been treated with 6-[(3-cyclobutyl-2,3,4,5-tetrahydro-1*H*-3-benzazepin-7-yl)oxy]-*N*-methyl-3-pyridinecarboxamide hydrochloride (GSK189254) (pig 1), 7-[4-[4-(2,3-dichlorophenyl)piperazin-1-yl]butoxy]-3,4-dihydro-1*H*-quinolin-2-one (aripiprazole) (pig 2), and 3,5-dichloro-*N*-[(1-ethylpyrrolidin-2-yl)methyl]-2-hydroxy-6-methoxy-benzamide (raclopride), 3-(2-[4-(4-fluorobenzoyl)-1-piperidinyl]ethyl)-2,4(1*H*,3*H*)-quinazolin-2-one tartrate salt (kentanerin), 2-(5-methoxy-1*H*-indol-3-yl)-*N,N*-dimethylethanamine (MeO-DMT), 2-ethenyl-4-azabicyclo[2.2.2]oct-5-yl)- (6-methoxyquinolin-4-yl)-methanol (quinidine) (pig 3) at pharmacologically active doses, in the hours prior to scanning with [ $^{11}\text{C}$ ]ROMAO (**4** or **5**). The fourth pig was dedicated to the [ $^{11}\text{C}$ ]ROMAO (**4** or **5**) study. After acquisition of a brief attenuation scan, 90 min long dynamic emission recordings were performed in the aperture of the Siemens ECAT Exact

tomograph. Pig 4 was scanned with *R*-[ $^{11}\text{C}$ ]ROMAO (**4**) before and after blocking with pargyline. Blood samples were collected during scans for pigs 2, 3, and 4 for metabolite measurements.

**Radiochemistry.** Acetonitrile (HPLC), dichloromethane, iodine, sodium phosphate monohydrate, and bufotenine (1 mg/mL) in acetonitrile were purchased from Bie and Berntsen, Denmark. Pargyline HCl, were obtained from Sigma–Aldrich, Denmark. The synthetic route to obtain (*R*)-(–) and (*S*)-(+)-1-(1-[ $^{11}\text{C}$ ]methyl-1*H*-pyrrol-2-yl)-2-phenyl-2-(pyrrolidin-1-yl)ethanone *R*- and *S*-[ $^{11}\text{C}$ ]ROMAO **4** and **5** is shown in Scheme 3. [ $^{11}\text{C}$ ]Carbon dioxide was prepared by a General Electric Medical Systems PET trace 200 cyclotron by a  $^{14}\text{N}(p,\alpha)^{11}\text{C}$  nuclear reaction. [ $^{11}\text{C}$ ]carbon dioxide was reduced to [ $^{11}\text{C}$ ]methane, which was then converted to [ $^{11}\text{C}$ ]methyl iodide using the General Electric methyl iodide box. The [ $^{11}\text{C}$ ]methyl iodide (6–9 GBq after 30 min of bombardment at 40  $\mu\text{A}$ ) was transferred in a stream of nitrogen and bubbled through the reaction mixture in a capped vial via a needle and vent needle. The premade reaction mixture was a suspension containing the precursor (**6** or **7**, ca. 1.5 mg) and NaH (0.3 mg) in DMF (300  $\mu\text{L}$ ); it was shaken before the [ $^{11}\text{C}$ ]methyl iodide gas was bubbled through it. The reaction mixture was left for 1 min at room temperature before it was quenched with HPLC eluent (0.3 mL) and transferred into the HPLC loop.

The reaction mixture was purified using a semipreparative HPLC (PerkinElmer model 200) equipped with a 5 mL injection loop. Product elution was monitored with online  $\gamma$  detection of in-house design, in conjunction with UV-visible detection (Applied Biosystems model 759A,  $\lambda = 300$  nm). The mobile phase, consisting of 30–40% ammonium formate (0.1 M, pH adjusted to 8.5 with NaOH) and 60–70% acetonitrile, was delivered at a rate of 10 mL/min to a SpherClone ODS (2) column. In both cases, the products eluted as broad peaks: the first one has  $R_f$  of 10–16 min (40% acetonitrile), and the second one has  $R_f$  of 25–32 min (30% acetonitrile). The fraction corresponding to the labeled product (ca. 25 mL) was collected, concentrated to ca. 5 mL under reduced pressure at 90 °C, and formulated with isotonic saline solution (5 mL).

The purity of the final product was determined by HPLC, using a BondClone C18 column (5  $\mu\text{m}$ ,  $250 \times 4.6$  mm) with an eluent consisting of 50% aqueous 0.1 M ammonium formate (pH 8.5 with NaOH) and 50% acetonitrile, with serial UV (250 nm) and  $\gamma$  detection. Reference standards of ROMAO (50  $\mu\text{g}/\text{mL}$ ) (**2** or **3**) and desmethyl-ROMAO (**6** or **7**) (50  $\mu\text{g}/\text{mL}$ ) were used for quantification. The product solution was spiked with ROMAO (**2** or **3**) in a second run to verify product identity on the basis of the co-elution position of the UV peak and the radioactivity peaks.

**Pharmacokinetic Analysis.** No arterial input was obtained for pigs 1–3; therefore, the analysis of tracer uptake in these three pigs were limited to the comparison of the region of interest (ROI) analysis of the summation images. For pig 4, continuous arterial inputs of untransformed *R*-[ $^{11}\text{C}$ ]ROMAO (**4**) and the sum of its metabolites were calculated. The area under the curve for plasma *R*-[ $^{11}\text{C}$ ]ROMAO (**4**) as a percentage of the total injected dose was calculated for the interval of the PET recording (90 min). Plasma metabolite analysis in pigs 3 and 4 was made from arterial blood samples (1 mL) drawn at 0.5, 2, 5, 10, 20, 30, 40, 50, 70, and 90 min after injection. The blood samples were centrifuged (1300g) for 1 min, and then 0.5 mL of the plasma was denatured by mixing with 0.5 mL of acetonitrile. The mixture was shaken and then centrifuged (1300 g) for 5 min. The supernatants were analyzed using a BondClone C18 column (5  $\mu\text{m}$ ,  $250 \times 4.6$  mm) with an eluent consisting of 50% aqueous 0.1 M ammonium formate (pH 8.5 with NaOH) and 50% acetonitrile, with serial UV (280 nm) and  $\gamma$  detection at a flow rate of 2.5 mL/min. The radioactivity of the precipitate was measured in a well counter cross-calibrated to the tomograph.

Voxel-wise parametric maps of the distribution volume ( $V_d$ , mL/g) of *R*-[ $^{11}\text{C}$ ]ROMAO (**4**) were calculated in the native PET space relative to the metabolite-corrected arterial input by the method of Turkheimer et al.<sup>29</sup> for pig 4. In this method, Akaike-weighted averages of the estimates of  $V_d$  for one- and two-tissue compartment

models were obtained in each voxel using linearized equations.<sup>30</sup> The sum of all emission frames from each PET session was calculated and manually registered to the MR-based common stereotaxic space for the minipig brain,<sup>29</sup> using a rigid-body transformation with 9 degrees of freedom in "Register".<sup>31</sup> Visual inspection of the individual dynamic and summed emission recordings did not reveal discernible head movement in the course of each PET session. Therefore, individual parametric maps of  $V_d$  were resampled into the common stereotaxic space using the transformation matrix and averaged by condition.

**Acknowledgment.** This project was supported by the Italian MUR and Denmark's National Science Foundation.

**Supporting Information Available:** Analytical data on compounds 6–8 and experimental data on animal handling. This material is available free of charge via the Internet at <http://pubs.acs.org>.

## References

- Schoepp, D. D.; Azzaro, A. J. Specificity of endogenous substrates for types A and B monoamine oxidase in rat striatum. *J. Neurochem.* **1981**, *36*, 2025–2031.
- Youdim, M. B. Monoamine oxidase. Its inhibition. *Mod. Probl. Pharmacopsychiatry* **1975**, *10*, 65–88.
- MacGregor, R. R.; Halldin, C.; Fowler, J. S.; Wolf, A. P.; Arnett, C. D.; Langström, B.; Alexoff, D. Selective, irreversible in vivo binding of [<sup>11</sup>C]clorgyline and [<sup>11</sup>C]-L-deprenyl in mice: potential for measurement of functional monoamine oxidase activity in brain using positron emission tomography. *Biochem. Pharmacol.* **1985**, *34*, 3207–3210.
- Fowler, J. S.; MacGregor, R. R.; Wolf, A. P.; Arnett, C. D.; Dewey, S. L.; Schlyer, D.; Christman, D.; Logan, J.; Smith, M.; Sachs, H.; Aquilonius, S. M.; Bjurling, P.; Halldin, C.; Hartvig, P.; Leenders, K. L.; Lundqvist, H.; Orelund, L.; Stalacke, C. G.; Langström, B. Mapping human brain monoamine oxidase A and B with <sup>11</sup>C-labeled suicide inactivators and PET. *Science* **1987**, *235*, 481–485.
- Arnett, C. D.; Fowler, J. S.; MacGregor, R. R.; Schlyer, D. J.; Wolf, A. P.; Långström, B.; Halldin, C. Turnover of brain monoamine oxidase measured in vivo by positron emission tomography using L-[<sup>11</sup>C]deprenyl. *J. Neurochem.* **1987**, *49*, 522–527.
- Lammersma, A. A.; Bench, C. J.; Price, G. W.; Cremer, J. E.; Luthra, S. K.; Turton, D.; Wood, N. D.; Frakowiak, R. S. J. Measurement of cerebral monoamine oxidase B activity using L-[<sup>11</sup>C]deprenyl and dynamic positron emission tomography. *J. Cereb. Blood Flow Metab.* **1991**, *11*, 545–556.
- Fowler, J. S.; Wolf, R. R.; MacGregor, R. R.; Dewey, S. L.; Logan, J.; Schlyer, D. J.; Langstrom, B. Mechanistic positron emission tomography studies: Demonstration of a deuterium isotope effect in the monoamine oxidase catalyzed binding of [<sup>11</sup>C]-L-deprenyl in living baboon brain. *J. Neurochem.* **1988**, *51*, 1524–1534.
- Fowler, J. S.; Wang, G. J.; Logan, J.; Xie, S.; Volkow, N. D.; MacGregor, R. R.; Schlyer, D. J.; Pappas, N.; Alexoff, D. L.; Patlak, C.; Wolf, A. P. Selective reduction of radiotracer trapping by deuterium substitution: Comparison of carbon-11-L-deprenyl and carbon-11-deprenyl-D2 for MAO B mapping. *J. Nucl. Med.* **1995**, *36*, 1255–1262.
- Logan, J.; Fowler, J. S.; Ding, Y. S.; Franceschi, D.; Wang, G. J.; Volkow, N. D.; Felder, C.; Alexoff, D. Strategy for the formation of parametric images under conditions of low injected radioactivity applied to PET studies with the irreversible monoamine oxidase A tracers [<sup>11</sup>C]clorgyline and deuterium-substituted [<sup>11</sup>C]clorgyline. *J. Cereb. Blood Flow Metab.* **2002**, *22*, 1376–1376.
- Ohmomo, Y.; Hirata, M.; Murakami, K.; Magata, Y.; Tanaka, C.; Ypkoyama, A. Synthesis and characterization of <sup>11</sup>C-labeled fluoroclogyline—A monoamine oxidase-A specific inhibitor for positron emission tomography. *Chem. Pharm. Bull.* **1993**, *41*, 1994–1997.
- Mukherjee, J.; Yang, Z.-Y. Development of N-[3-(2',4'-dichlorophenoxy)-2-<sup>18</sup>F-fluoropropyl]-N-methylpropargylamine (<sup>18</sup>F-fluoroclogyline) as a potential PET radiotracer for monoamine oxidase-A. *Nucl. Med. Biol.* **1999**, *26*, 619–625.
- Mukherjee, J.; Yang, Z.-Y. Monoamine oxidase A inhibition by fluoxetine: an in vitro and in vivo study. *Synapse* **1999**, *31*, 285–289.
- Hamid, R.; Chalou, S.; Ombetta, J.-E.; Frangin, Y.; Garreau, L.; Dognon, A.-M.; Lena, I.; Bodard, S.; Vilar, M.-P.; Besnard, J.-C.; Guilloteau, D. Synthesis and characterization of [<sup>125</sup>I]N-(2-aminoethyl)-4-iodobenzamide as a selective monoamine oxidase B inhibitor. *Nucl. Med. Biol.* **1995**, *22*, 617–623.
- Bergström, M.; Westerberg, G.; Långström, B. <sup>11</sup>C-Harmine as a tracer for monoamine oxidase A (MAO-A): In vitro and in vivo studies. *Nucl. Med. Biol.* **1997**, *24*, 287–293.
- Bergström, M.; Westerberg, G.; Nemeth, G.; Traut, M.; Gross, G.; Greger, G.; Müller-Peltzer, H.; Safer, A.; Eckernäs, S.-Å.; Grahn, A.; Långström, B. MAO-A inhibition in brain after dosing with esuprone, moclobemide, and placebo in healthy volunteers: In vivo studies with positron emission tomography. *Eur. J. Clin. Pharmacol.* **1997**, *52*, 121–128.
- Jensen, S. B.; Olsen, A. K.; Pedersen, K.; Cumming, P. Effect of monoamine oxidase inhibition on amphetamine-evoked changes in dopamine receptor availability in the living pig: A dual tracer PET study with [<sup>11</sup>C]harmine and [<sup>11</sup>C]raclopride. *Synapse* **2006**, *59*, 427–434.
- Meyer, J. H.; Ginovart, N.; Boovariwala, A.; Sagrati, S.; Hussey, D.; Garcia, A.; Young, T.; Prashak-Rieder, N.; Wilson, A. A.; Houle, S. Elevated monoamine oxidase A levels in the brain—An explanation for the monoamine imbalance of major depression. *Arch. Gen. Psychiatry* **2006**, *63*, 1209–1216.
- Bottlaender, M.; Dolle, F.; Guenther, I.; Roumenov, D.; Fuseau, C.; Barmouille, Y.; Curet, O.; Jegham, J.; Pinquier, J. L.; Valette, G. P. Mapping the cerebral monoamine oxidase type A: Positron emission tomography with the reversible selective inhibitor [<sup>11</sup>C]befloxatone. *J. Pharmacol. Exp. Ther.* **2003**, *305*, 467–473.
- Dolle, F.; Valette, H.; Barmouille, Y.; Guenther, I.; Fuseau, C.; Coulon, C.; Lartizien, C.; Jegham, S.; George, P.; Curet, O.; Pinquier, J. L.; Bottlaender, M. Synthesis and in vivo imaging properties of [<sup>11</sup>C]befloxatone: A novel highly potent positron emission tomography ligand for mono-amine oxidase-A. *Bioorg. Med. Chem. Lett.* **2003**, *13*, 1771–1775.
- Fowler, J. S.; Volkow, N. D.; Wang, G. J.; Pappas, N.; Logan, J.; Shea, C.; Alexoff, D.; MacGregor, R. R.; Schlyer, D. J.; Zezulkova, I.; Wolf, A. P. Brain monoamine oxidase A inhibition in cigarette smokers. *Proc. Natl. Acad. Sci. U.S.A.* **1996**, *93*, 14065–14069.
- Fowler, J. S.; Volkow, N. D.; Wang, G. J.; Pappas, N.; Logan, J.; MacGregor, R.; Alexoff, D.; Wolf, A. P.; Warner, D.; Cilento, R.; Zezulkova, I. Neuropharmacological actions of cigarette smoke: Brain monoamine oxidase B (MAO B) inhibition. *J. Addict. Dis.* **1998**, *17*, 23–34.
- Basford, R. E. Preparation and properties of brain mitochondria. *Methods Enzymol.* **1967**, *10*, 96–101.
- Di Santo, R.; Costi, R.; Roux, A.; Artico, M.; Befani, O.; Meninno, T.; Agostinelli, E.; Palmegiani, P.; Turini, P.; Cirilli, R.; Ferretti, R.; Gallinella, B.; La Torre, F. Design, synthesis, and biological activities of pyrrolylethanoneamine derivatives, a novel class of monoamine oxidase inhibitors. *J. Med. Chem.* **2005**, *48*, 4220–4223.
- Lind, N. M.; Moustgaard, A.; Jelsing, J.; Vajta, G.; Cumming, P.; Hansen, A. K. The use of pigs in neuroscience: Modeling brain disorders. *Neurosci. Biobehav. Rev.* **2007**, *31* (5), 728–751.
- Pedersen, K.; Simonsen, M.; Ostergaard, S. D.; Munk, O. L.; Rosa-Neto, P.; Olsen, A. K.; Jensen, S. B.; Moller, A.; Cumming, P. Mapping the amphetamine-evoked changes in [<sup>11</sup>C]raclopride binding in living rat using small animal PET: Modulation by MAO inhibition. *Neuroimage* **2007**, *35* (1), 38–46.
- Jensen, S. B.; Smith, D. F.; Bender, D.; Jakobsen, S.; Peters, D.; Nielsen, E. O.; Olsen, G. M.; Scheel-Kruger, J.; Wilson, A.; Cumming, P. [<sup>11</sup>C]-NS 4194 versus [<sup>11</sup>C]-DASB for PET imaging of serotonin transporters in living porcine brain. *Synapse* **2003**, *49*, 170–177.
- La Torre, F.; Cirilli, R.; Costi, R.; Di Santo, R.; Ferretti, R.; Gallinella, B.; Salerno, A.; Zanitti, L. Enantiomers of new synthetic pyrrolylethanoneamine mono-amino oxidase inhibitor compounds: Analytical and semipreparative HPLC separations, and chiroptical characteristics. *Chromatographia* **2004**, *60*, 171–178.
- Cumming, P.; Yokoi, F.; Chen, A.; Deep, P.; Dagher, A.; Reutens, D.; Kapczynski, F.; Wong, D. F.; Gjedde, A. Pharmacokinetics of radiotracers in human plasma during positron emission tomography. *Synapse* **1999**, *34*, 124–134.
- Turkheimer, F. E.; Hinz, R.; Cunningham, V. J. On the undecidability among kinetic models: From model selection to model averaging. *J. Cereb. Blood Flow Metab.* **2003**, *23*, 490–498.
- Zhou, Y.; Brasic, J. R.; Ye, W.; Dogan, A. S.; Hilton, J.; Singer, H. S.; Wong, D. F. Quantification of cerebral serotonin binding in normal controls and subjects with Tourette's syndrome using [<sup>11</sup>C]MDL 100,907 and (+)[<sup>11</sup>C]McN 5652 dynamic PET with parametric imaging approach. *Neuroimage* **2004**, *22*, T98–T99.
- MacDonald, D. *Program for Registration of Images (Register)*; McConnell Brain Imaging Center: Montreal, Canada, 1986.